BNL-209671-2018-JAAM

# Highly Dispersed Carbon Supported PdNiMo Core with Pt Monolayer Shell Electrocatalysts for Oxygen Reduction Reaction

C. Okoli, K. Sasaki

To be published in "ECS Transactions "

November 2018

Chemistry Department

**Brookhaven National Laboratory**

**U.S. Department of Energy**

USDOE Office of Science (SC), Basic Energy Sciences (BES) (SC-22)

# DISCLAIMER

# Highly Dispersed Carbon Supported PdNiMo Core with Pt Monolayer Shell Electrocatalysts for Oxygen Reduction Reaction

Celest Okoli[a, b], Kurian A. Kuttiyiel[c], Kotaro Sasaki*[, c], Dong Su[d], Debasish Kuila[e], Devinder Mahajan*[, a, b], Radoslav R. Adzic[b, c]

[a] Advanced Energy Research and Technology Center, Stony Brook University, Stony Brook, NY
[b] Materials Science & Chemical Engineering Department, Stony Brook University, Stony Brook, NY
[c] Chemistry Department, Brookhaven National Laboratory, Upton, NY
[d] Center for Functional Nanomaterials, Brookhaven National Laboratory, Upton, NY 11973
[e] Department of Chemistry, North Carolina Agriculture and Technical State University, Greensboro, North Carolina 27411

## Abstract

The development of low-cost, durable, and high-performance materials that could substitute for the current platinum-based electrocatalysts would accelerate the commercialization of polymer electrolyte membrane fuel cells as an alternative power source. We report herein a new fabrication approach of carbon-supported platinum monolayer (ML) on ternary palladium-nickel-molybdenum core electrocatalysts ($Pt_{ML}$/PdNiMo/C) by a sonochemical method using ionic liquid (IL) as a dispersion medium. The sonolysis technique can control the size and distribution of the ternary-metal nanoparticles on different carbon supports without addition of any external reducing agents, surfactants or capping agents. Depositing Pt MLs using under-potential deposition method on the ternary PdNiMo nanoparticle cores could enhance activity and durability of the cathode during the oxygen reduction reaction of the fuel cell. Herein, we show that the described sonolysis method produces more reliable and cost-effective electrocatalysts that outperforms a commercial Pt-based catalyst.

Key words: Sonolysis, electrocatalysts, nanoparticles (NP), ionic liquid, oxygen reduction

## Introduction

It is widely known that electrochemical energy conversion and storage systems such as fuel cells, electrolyzers and supercapacitors can serve as viable paths to energy sustainability. However, the low performance and high cost of most of these systems remain a major obstacle for their full commercialization. The performance of these systems depends largely on the properties of the materials used in the electrode, which is one of the most vital components (1). In proton exchange membrane fuel cells (PEMFCs) that use hydrogen as a fuel, platinum (Pt) has been the dominant choice for both the cathode and the anode, but the high cost and content of Pt particularly at the cathode resulting from sluggish oxygen reduction reaction (ORR) and poor stability, are some of the challenges facing its commercial viability (2). Therefore, the most recent research effort is focused on reducing the Pt content through synthesis of Pt-based alloys and Pt core-shell electrocatalysts.

Several techniques to fabricate electrocatalysts and their support materials for fuel cell applications have been developed. Most of these techniques have inherent limitations such as high costs, severe synthesis conditions involving high vacuum and high temperature, long durations, and safety issues. The synthesis of metal/bimetal nanoparticles (NPs) on carbon supports have been widely studied; several synthetic methods have emerged, such as chemical reduction (2-7), electrochemical reduction (4, 8), photochemical reduction (4), microwave (1, 8), gas-phase sputtering (8), and physical vapor deposition (4, 8). In most chemical methods, the use of some reducing agents or solvents makes the process unacceptable due to the associated environmental problems for mass production. Most other methods are either too expensive or have other mass production issues.

Recently, a sonochemical technique, which utilizes a cavitation phenomenon induced by irradiation of high-intensity ultrasound, has been paid attention as a facile method to synthesize various forms of NPs. Suslick *et al*. synthesized monometallic and bimetallic nanoparticles by high intensity ultrasound at low temperatures (9). The bimetallic NPs in which they have synthesized have various forms including solid solution, core-shell, and segregated two-phase structures. However, the stability of the bimetallic nanomaterials seemed unsatisfactory. Mizukoshi *et al*. (10) reported the preparation of Au@Pd core-shell NPs by sonochemical reduction, simultaneously applied in an aqueous solution containing $Au^{3+}$ and $Pd^{2+}$ ions, and the thickness of a Pd shell and the size of Au core may depend on the ratio of added concentration of the ions.

As for ternary NP synthesis, the formation of solid solution alloys were not guaranteed due to many factors such as different reaction kinetics and surface free energies of the metals that contribute to the final product formation. When an immiscible mixture of metals is used, alloy formation is unlikely, and the formation of core-shell, fused cluster, and NPs depend on the reaction kinetics and surface interactions with the surrounding medium (10). Other researchers such as Manthiram *et al*. (11) and Yoon *et al*. (12) prepared PdMo electrocatalysts for the methanol oxidation reaction and the oxygen reduction reaction in fuel cells, respectively. The synthesis methods used were either thermal decomposition of palladium acetylacetonate and molybdenum hexacarbonyl precursors at very high temperatures or by hydrothermal decomposition in different pH. In these studies, the high temperature used during synthesis resulted in large sized nanoparticles and moderate stability of the final products in alkaline media, but highly unstable in acidic media of PEMFC. Furthermore, since one of the primary functions of electrodes is to convert ionic conductivity into electrical conductivity; electrode materials

should have intrinsic properties. Using ionic liquid in the synthesis has achieved that objective as presented by Dupont and coworkers (3, 13) in their studies on synthesis of transition metal nanoparticle catalysts in which they generated small size nanoparticles, with narrow size distribution and different shapes. The process is scalable because very small quantity of ionic is needed and most of the ionic liquid is recovered and recycled (14).

Janiack (8) provided a comprehensive review on the synthesis and stabilization of metal nanoparticles, while Kraynov and Muller (4) investigated the stabilization mechanism through modeling. None of these mentioned studies that produced electrocatalysts with good stability for electrochemical applications used mild or green solvents. Recently, we described sonochemical synthesis of metal alloy nanoparticles in different solvents as electrocatalysts with improved catalytic activity (15). In the study, we observed that ionic liquid and solvents used have significant influence on the size, shape and dispersion of synthesized nanoparticles. Based on our previous work, we developed ternary PdNiMo alloy nanoparticles to provide a stable core support for Pt monolayer electrocatalysts.

## 2. Experimental

### *2.1. Materials*

Molybdenum hexacarbonyl ($Mo(CO)_6$), palladium acetylacetonate ($Pd(acac)_2$), bis(1,5-cyclooctadiene)nickel ($Ni(COD)_2$), benzoic acid ($C_7H_6O_2$) were purchased from Sigma Aldrich, while an ionic liquid (IL), tributyl-methyl phosphonium bis(trifluoromethylsulfonyl)imide (TBPh $Tf_2N$) was purchased from Iolitec Inc.

### *2.2. Sonochemical synthesis of PdNiMo nanoparticles on IL functionalized carbon.*

60 mg of Vulcan XC72R carbon was mixed with 15 ml of TBPh $Tf_2N$, and the mixture was ground using a mortar for 20 min to form a black paste. The paste was centrifuged twice at 9000 rpm for 30 min to separate the carbon from IL. The resulting paste was washed thoroughly with a 1:1 ratio of acetonitrile and deionized (DI) water before drying in a vacuum oven at 40°C for 2 days. The recovered IL was recycled twice in subsequent paste preparation. The IL functionalized carbon (236 mg) was placed in 70 ml of ethanol / DI water (1:1) solvent. Previous studies have shown that addition of benzoic acid acts as a modulator to promote the formation of defects that can enhance the reactivity of materials (16, 17). Therefore, 1 g of benzoic acid was added to the solution to promote the yield and Ni deposition. The slurry was purged with $N_2$ gas for 20 min, and $Pd(acac)_2$, $Ni(COD)_2$, and $Mo(CO)_6$ precursors were added to the slurry. The total metal loading was 30 wt-%. The solution was purged again with $N_2$ gas for 10 min before sonolysis. The sonochemical treatments were carried out using an ultrasonic liquid processor Misonix 3000 with variable power up to 200 W at a fixed frequency of 20 kHz. The sonolysis processes were monitored through carbon monoxide (CO) gas evolution, and the power of 81W was on average required at 40 ºC for 0.5 h to achieve full decomposition of the metal precursors. The collected gas during sonolysis was analyzed using Gow-Mac 580 gas chromatograph fitted with a molecular sieve column under helium flow. We noted that inert nitrogen gas, carbon monoxide from carbonyls and some from the IL, contributed to the observed gases from analysis.

The product was separated by centrifugation, washed two times with acetone and deionized water, and dried in a vacuum oven at 40 °C for 24 h. The carbon-supported PdNiMo NPs were then annealed at 200 ºC in a 5% $H_2$/Ar gas for 3 h.

*2.3. Electrochemical measurements*

Electrochemical measurements were carried out with a Biologic potentiostat and a three-electrode cell. The PdNiMo/C electrocatalyst was dispersed in a water/isopropyl alcohol mixed solution by sonication to give a content of 1 mg/ml. A catalyst ink/dispersion was dropped on a glassy carbon rotating disk (RDE) electrode as the working electrode. The electrode was then covered by a small amount of a Nafion solution (5 μL of 4 μg/10 μL) and dried in air. We deposited Pt monolayer on the prepared PdNiMo/C surfaces using the galvanic displacement of Cu layer formed by Cu under-potential deposition (UPD) (18). A Pt wire was used as a counter electrode, and Ag/AgCl/KCl (3M) electrode with double junction as a reference electrode. All potentials presented are quoted versus a reversible hydrogen electrode (RHE). Cyclic voltammograms (CVs) were recorded between 0.0 to 1.1V with a scanning rate of 20 mV $s^{-1}$ in an Ar-saturated 0.1 M $HClO_4$ solution. ORR polarization curves were recorded using the RDE in $O_2$-saturated 0.1 M $HClO_4$ electrolyte at rotation rates from 400 to 2500 rpm at a sweep rate of 10 mV $s^{-1}$. Stability tests for the electrocatalysts were conducted in air-saturated 0.1 M $HClO_4$, with a potential range between 0.6 and 1.0 V at a sweep rate of 50 mV $s^{-1}$ at room temperature for 8,000 cycles. A commercial E-TEK Pt/C catalyst with a particle size of 3.2 nm was used for comparison.

### *2.4 Characterization*

The Hitachi aberration-corrected scanning transmission electron microscope (STEM), equipped with a high resolution Gatan Enfina electron energy loss spectrometer (EELS) at the Center for Functional Nanomaterial (CFN), Brookhaven National Laboratory (BNL), was used to characterize the PdNiMo/C electrocatalysts. The STEM imaging and EELS data were collected using 1.3 Å electron probe with a probe current of 50 pA. The STEM convergence and collection angles were 28 mrad and 114 - 600 mrad respectively. The contrast of the images directly related

with atomic number (Z-contrast), while the EELS energy of resolution was about 0.4 eV as estimated from the half with of zero loss peaks.

*Ex situ* XRD experiments were performed at the XPD beamline at NSLS-II. The XRD spectra were recorded using a 2D detector (Perkin Elmer XRD 1621 N ES) at 12.4 keV and subsequently processed using standard data processing software. The dark current and the diffraction pattern were collected over 40 seconds (10 exposures at 4 s each) and the diffraction pattern was recorded over 400 seconds (100 exposures at 4 s per exposure). The wavelength of X-ray used was 0.18351 Å.

X-ray absorption spectroscopy (XAS) measurements were undertaken at the BL 2-2 beamline at the Stanford Synchrotron Radiation Lightsource (SSRL), SLAC National Accelerator Laboratory. The *ex situ* measurements were carried out at the Pd K edge (24350 eV), Mo K edge (20000 eV) and Ni K edge (8333 eV) at room temperature. The XAS data were acquired in both the transmission and fluorescence modes. The data acquired were processed and analyzed by Athena and Artemis software (19).

## 3. Results and discussion

### *3.1 Morphology and Structure*

Figure 1 shows the high angle annular dark field (HAADF) HRTEM images of the PdNiMo/C nanoparticles, which are almost spherical with a mean particles size of 4.1 nm (Figure S3). As shown in Figure 1a, most of the nanoparticles were between 2.5 nm and 6 nm in size. The IL introduces a large number of active sites on the carbon surfaces for the nucleation and growth of nanoparticles (20). The physical interactions of the IL with surfaces of carbon not only serve

as dispersion and functionalization agents but also allow the metal precursors to interact electrostatically with the IL ions (*i.e.* TBPh $Tf_2N$ anions) that need to bond to the surfaces of the carbon material (21). Thus, it is considered that the IL used for the functionalization of carbon provides ideal templates for the deposition and dispersion of PdNiMo nanoparticles. The composition of the PdNiMo nanoparticles was identified by energy dispersive X-ray (EDX) measurements. The Pd, Ni and Mo contents were 19 wt-%, 7 wt-% and 4 wt-% respectively. We note that the composition of prepared PdNiMo nanoparticles can be controlled by changing the ratio of concentrations of the precursors.

A comparison of the EELS intensities (Figure 1d) for the Pd M-edge, Ni L-edge and Mo L-edge on a PdNiMo nanoparticle was obtained by moving the electron probe along the line indicated in Figure 1c (we note on the arbitrary scales of the y axis). The intensities of both Mo and Ni are the highest around x=3.8 nm and become lower toward to both edge of the nanoparticle, while the intensity of Pd shows a more uniform distribution over the particle compared with other two elements.

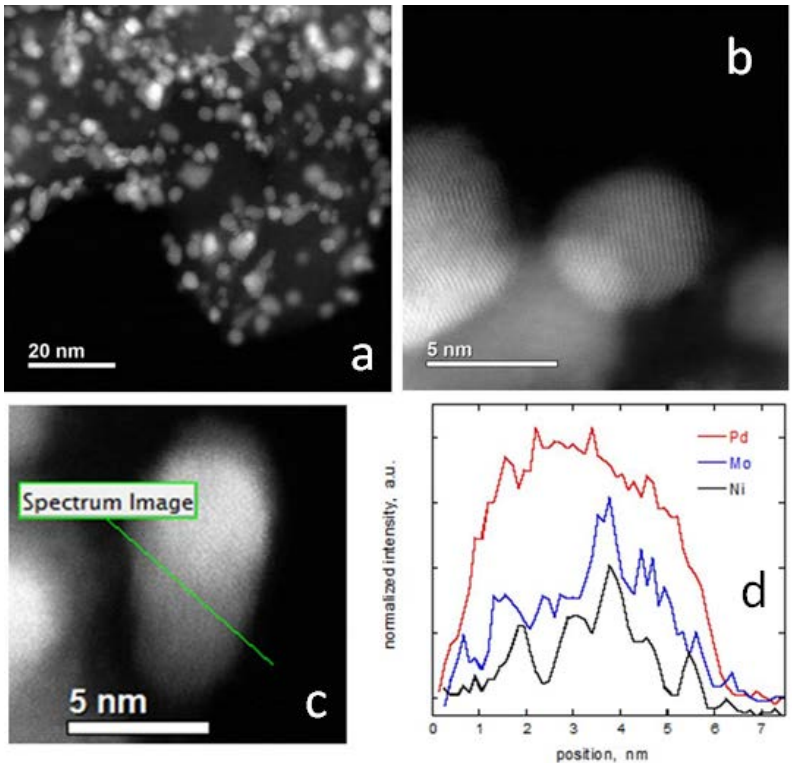


Figure 1. (a, b) HAADF-STEM images of PdNiMo nanoparticles. (d) EELS line-scan profiles of Pd M edge, Mo L edge, and Ni L edge scanned along the line as indicated in (c) HAADF-STEM image of a single nanoparticle.

The synchrotron XRD pattern of the PdNiMo /C catalysts is shown in Figure 2. The average particles diameter calculated from the Pd(1 0 0) peak using the Scherrer equation was 4.4 nm, which is in line with the result from HAADF-STEM observation. No clear individual peaks for Ni and Mo were observed on the XRD pattern. As discussed below, Ni and Mo are present as a form of oxides.

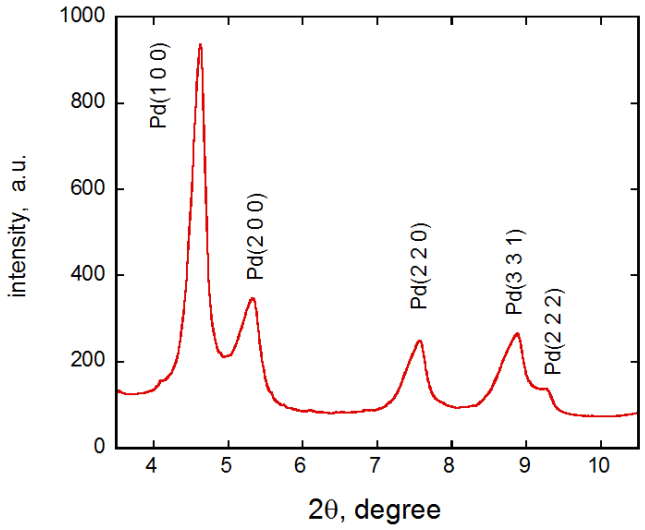


Figure 2. Synchrotron XRD pattern of PdNiMo/C. Wavelength: 0.1825 Å.

Figure 3 shows *ex situ* X-ray absorption near-edge structure (XANES) and the Fourier transformed (FT) extended X-ray absorption fine structure (EXAFS) spectra of the Pd K edge (24350 eV) (a, b), the Ni K edge (8331 eV) (c, d), and the Mo K edge (20000 eV) (e, f) from PdNiMo/C, together with their reference foils and oxides. Fig. 3a shows a slight difference between the Pd K edge XANES spectra from PdNiMo/C and a Pd foil. The intensity of the first peak of PdNiMo/C is a little lower than that of the foil. However, the difference is not due to oxidation of Pd in PdNiMo/C, but is caused by a change in the *d*-band electronic state in Pd due to the presence of Ni and/or Mo atoms (22). The FT EXAFS spectrum of Pd K edge from PdNiMo/C (Fig. 3b) is also dissimilar to that of the foil. In addition, in the spectrum in *k*-space from PdNiMo/C (Fig. S2), the phase in oscillation is slightly shifted compared with that from the foil (at $4 < k < 13$ Å$^{-1}$); these two spectra represent alloying of Pd with Ni and/or Mo to some degree. The Ni K edge XANES spectrum from PdNiMo/C (Fig. 3c) shows a strong white line signal at 8350 eV, which indicates the formation of Ni oxide in the PdNiMo nanoparticles. The FT EXAFS spectrum of Ni K edge from PdNiMo/C (Fig. 3d) is similar to that of NiO. The XANES

spectrum of Mo K edge from PdNiMo/C (Fig. 3e) is different from that of Mo foil. It shows a distinctive pre-edge peak, and a similar pre-peak is also seen in the spectrum of ammonium molybdate ($(NH_4)_2MoO_4$). Such a pre-peak is known to be the characteristic Mo(VI) species as a result of the dipole forbidden $1s \rightarrow 4d$ transitions (23), thus the oxidation state of Mo in PdNiMo/C could be 6. We note that similar XANES spectra of Ni and Mo K edges have been observed in NiMo nanoparticles synthesized by annealing in $H_2$ at 400 ºC in our previous study (24). We interpreted that the NiMo nanoparticles could have oxidized promptly after the annealing step. The annealing temperature for this study was 200°C in a 5% $H_2$/Ar gas, and it is also likely that Mo and Ni oxides were spontaneously formed while stored in air after the synthesis.

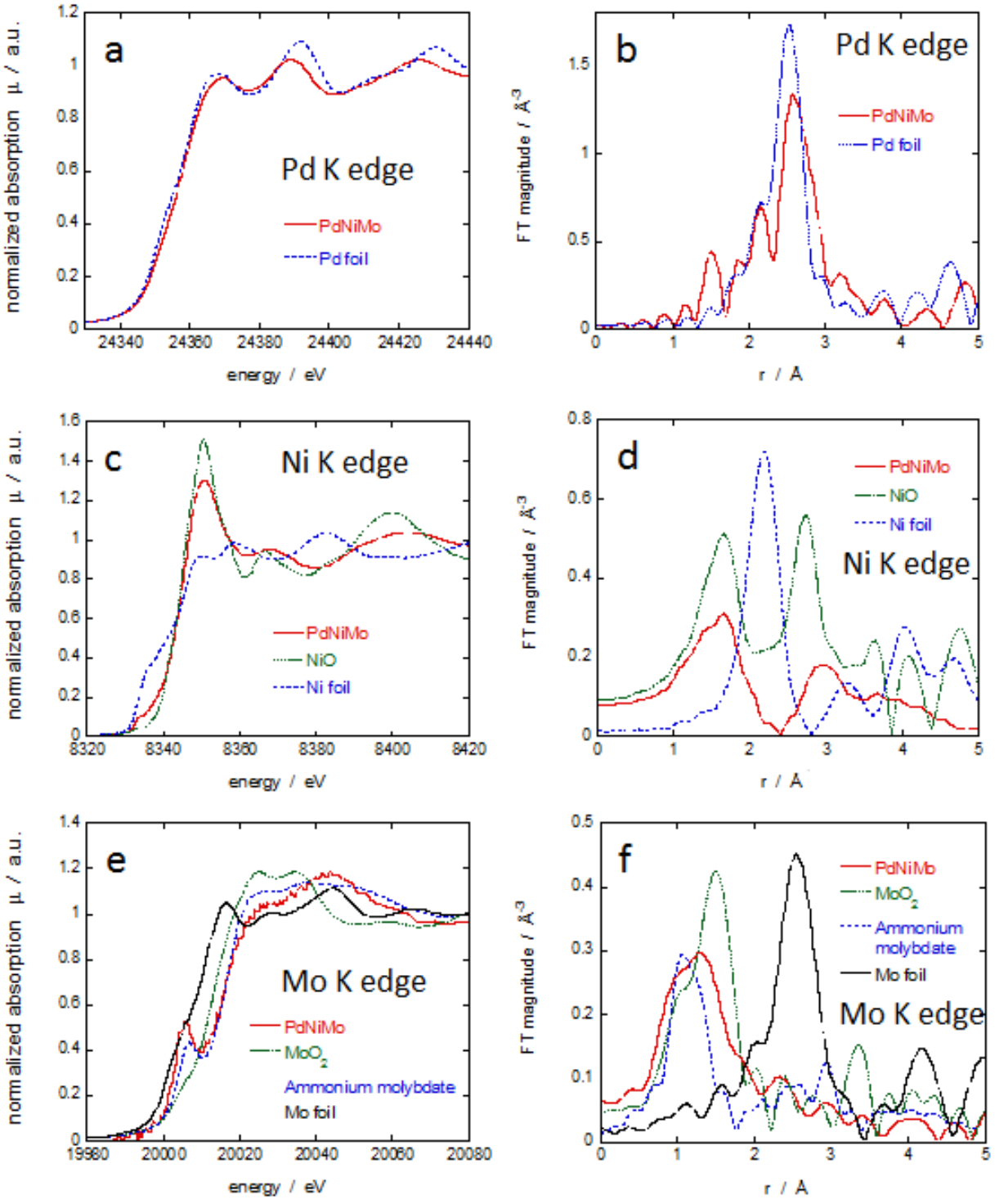


Figure 3. *Ex situ* XANES and the Fourier transformed (FT) EXAFS spectra of (a, b) the Pd K edge (24351 eV), (c, d) the Ni K edge (8331 eV), and (e, f) the Mo K edge (20000 eV) from PdNiMo/C, together with their reference foils and oxides.

We suggest a plausible mechanism for the formation of PdNiMo nanoparticles based on the decomposition reaction kinetics data and surface interactions with the surrounding medium during sonolysis. In the presence of $Tf_2N$ IL-functionalized carbon, it is possible that the $Tf_2N$ anion on carbon intervenes in the Ni(0) formation through interaction with the COD ligands, leading to the spontaneous decomposition of $Ni(COD)_2$ on carbon surfaces (25). Owing to the interaction between $Tf_2N$ anion and COD ligands, $Ni(COD)_2$ may decompose more rapidly than the deposition of Mo and Pd precursors. Then, the decomposition of $Mo(CO)_6$ through dissociation of carbonyl ligand and the reduction of $Pd(acac)_2$ by sonochemically generated hydrogen radicals (26) occur preferentially on the surface of nickel nuclei that have already been formed.

*3.2. Electrochemical ORR activity and stability*

Platinum monolayers were deposited on the surfaces of PdNiMo/C nanoparticles by replacing underpotentially deposited copper monolayers. The cyclic voltammetry (CV) curves were generated for $Pt_{ML}$/PdNiMo/C and commercial Pt/C (E-TEK 10 wt-% Pt on Vulcan X72R) catalysts (Figure 4.1). The Pt loading for $Pt_{ML}$/PdNiMo/C and Pt/C catalyst based on the geometric electrode area of 0.196 $cm^2$ were 3.2 $\mu g/cm^2$ and 7.7 $\mu g/cm^2$, respectively. The oxide adsorption/desorption potentials observed from $Pt_{ML}$/PdNiMo/C shifted more positively (ca. 40 mV) in comparison with those from Pt/C, indicating a remarkable effect of the substrate on Pt atoms on the surfaces. Figure 4.1b shows a comparison of polarization curves for the ORR on $Pt_{ML}$/PdNiMo /C and commercial Pt/C electrocatalysts in oxygen-saturated 0.1 M $HClO_4$ at a rotation rate of 1600 rpm. It is clearly seen that the ORR activity of Pt/PdNiMo/C is much higher than that of Pt/C in spite of the lower Pt loading. The ORR curves of the $Pt_{ML}$/PdNiMo/C electrocatalyst at different rotation speeds (400 to 2500 rpm) in a 0.1 M $HClO_4$ solution purged by $O_2$ are shown in supplementary material (Figure 4e). Using the same data, the Koutecky-Levich

plot, *i.e.*, the inverse current ($1/I$) plotted as a function of inverse of square root of the rotation rate ($\omega^{1/2}$), is presented in Figure 4f. The linearity and parallelism of these plots indicate a first-order kinetics with respect to molecular oxygen (27). The kinetic currents for ORR can be determined from the intercepts of the $1/I$ axis at $\omega^{1/2} = 0$. The Pt specific and mass activities of the $Pt_{ML}$/PdNiMo/C electrocatalyst at 0.9 V were determined to be 0.55 $mA/cm^2$ and 1.14 $A/mg_{Pt}$, which are approximately 2.3 and 5.7 times higher than those of the commercial Pt/C electrocatalyst (0.24 $mA/cm^2$ and 0.2 $A/mg_{Pt}$). Its total platinum group metal (PGM) (Pt+Pd) mass activity is 0.21 $A/mg_{PGM}$, and the electrochemical surface area (ECSA) is 188 $m^2/g_{Pt}$. The enhancement in activity observed for the $Pt_{ML}$/PdNiMo/C catalyst can be explained in terms of electronic modifications of Pt surface atoms induced by strain, ligand and segregation effects in ternary PdNiMo surfaces (28). Even though the PGM mass activity of $Pt_{ML}$/PdNiMo/C is lower than that of the other $Pt_{ML}$ on ternary nanoparticle core catalyst such as $Pt_{ML}$/AuPdNi/C (0.53 $A/mg_{PGM}$) which was developed and reported earlier by our group (29), the stability and lower cost due to the absence of gold in the nanostructure of the present system is favorable.

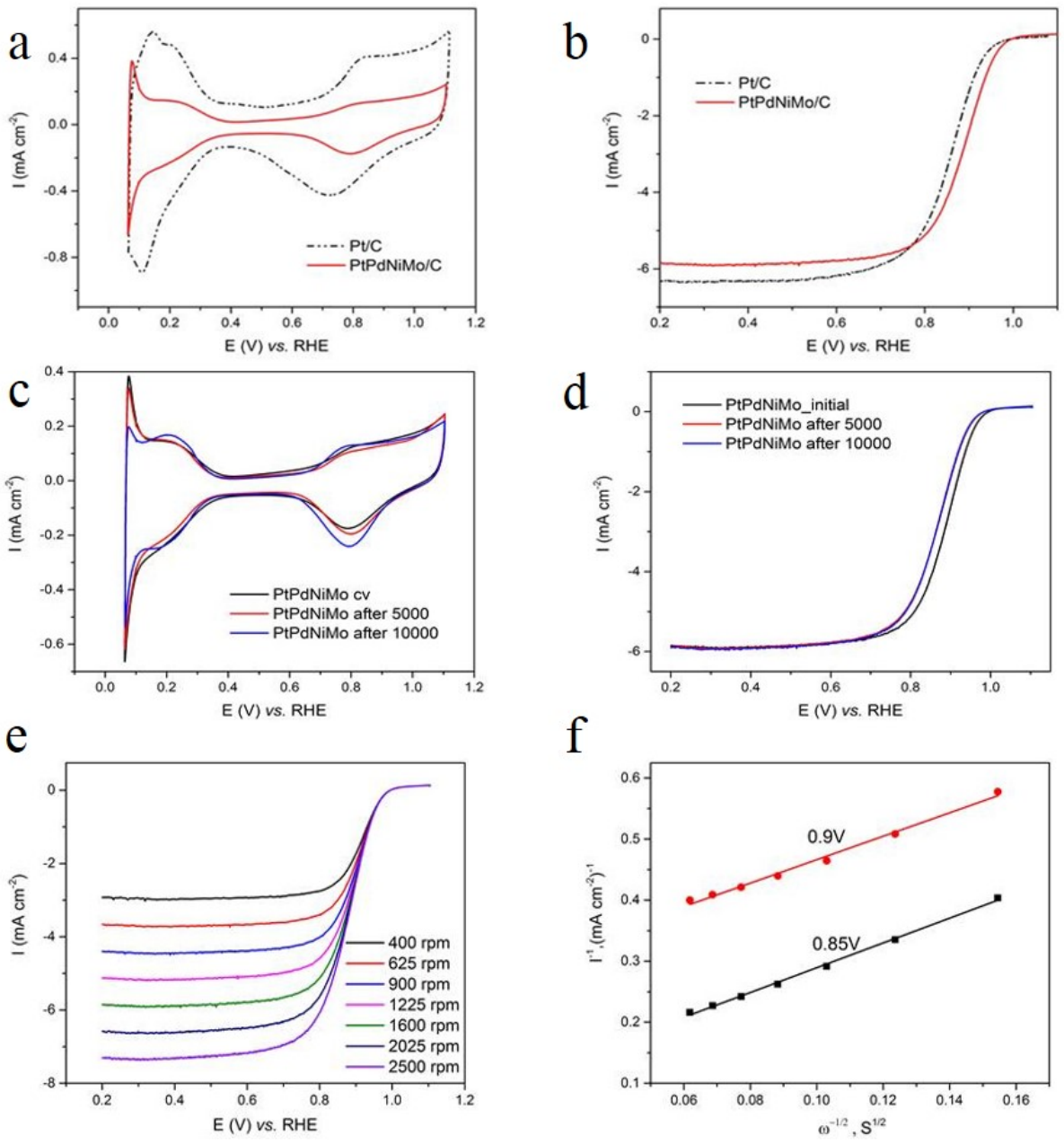


Figure 4. (a) A comparison of CV in Ar-saturated and (b) ORR Polarization curves at 1600 rpm in oxygen-saturated 0.1 M $HClO_4$ on thin-film electrodes for Pt/C and $Pt_{ML}$/PdNiMo/C respectively. (c, d) CV and ORR of $Pt_{ML}$/PdNiMo/C electrocatalyst after potential cycling test. (e, f) ORR curves on the $Pt_{ML}$/PdNiMo/C electrocatalyst at different rotation speeds (400 to 2500 rpm) in 0.1 M HClO4 along with its Koutecky-Levich plot at 0.9 and 0.85V.

Another important criterion in electrocatalysts design for fuel cells is the long-term stability. The accelerated stability tests for $Pt_{ML}$/PdNiMo/C were carried out by applying triangular sweeps between 0.6 V and 1.0V with a scan rate of 50 mV/s in an air-saturated 0.1M $HClO_4$ solution at room temperature. The initial half-wave potential ($E_{1/2}$) of PdNiMo/C was 888 mV and reduced to 869 mV after 10,000 cycles, whereas the specific and PGM mass activity dropped to 0.51 mA/cm$^2$ and 0.19 A/mg respectively. The ORR polarization curve showed only a decrease of 19 mV after cycling for 10,000 cycles, while the CVs exhibited nearly no loss in the hydrogen adsorption/desorption peaks (Figure 4c), and the results exhibited higher durability than commercially available Pt/C (30, 31), demonstrating that using this ternary nanostructured substrate as a core for Pt MLs also produces highly stable electrocatalysts.

Previous stability tests on the Pt ML on Pd core electrocatalyst ($Pt_{ML}$/Pd/C) demonstrated long-term stability (22, 32), and the EXAFS analysis showed that the Pt ML structure was almost retained after 60,000 potential cycles in MEA tests (32). Pd is a slightly more reactive metal than Pt with a lower standard electrochemical potential ($U_{Pd}^0$: 0.92 V), and thus Pd dissolution occurs at slightly lower potentials than Pt ($U_{Pt}^0$: 1.19 V). Owing to an exposure to fluctuating fuel-cell voltage, the Pd may be oxidized to $Pd^{2+}$ and diffuse through any imperfection (puncture) in a Pt ML. The preferential Pd oxidation presumably prevents the oxidation of Pt MLs and exerts a certain degree of cathodic protection on Pt MLs. If Pd oxidation/dissolution is effectively inhibited, the overall durability of the Pt ML catalyst will be further improved. We have previously demonstrated that adding a small amount of Au atoms (approximately 10 at-%) to Pd and forming highly uniform nanoparticle cores make corrosion-resistant PdAu nanoparticle cores, resulting in synthesizing the highly tolerant Pt ML electrocatalyst (22).

In the present study, we found that the addition of MoNi to Pd nanoparticles also retards Pd oxidation. Figures 5a and b show the *in situ* XANES and FT-EXAFS spectra of Pd K edge of the PdNiMo/C nanoparticles at different potentials (0.41 – 1.11 V), respectively. Both the XANES and FT-EXAFS of Pd K edge change only slightly with increasing potentials, which is different from those observed for a commercial Pd/C (Figure 5c) (22). In Figure 5c, the peak around 1.6 Å reflects the formation of Pd oxide on the Pd/C. Clearly, the oxidation of Pd of PdNiMo/C is significantly hampered and metallic Pd remained up to 1.11 V. We consider that the enhanced stability of Pd may be derived from the electronic effect of the alloying element Mo (rather than Ni), and the observation is supported by recent findings that addition of Mo to Pd inhibits Pd-O formation on the PdMo alloy nanoparticles (11, 12). The stable PdNiMo cores impart improved durability of Pt MLs, as reported in an earlier study of the $Pt_{ML}$/AuPd/C catalyst (22). The marked feature of the present study is that the highly stable $Pt_{ML}$/Pd-based-core catalyst has been developed by a sonochemical method, without the inclusion of an expensive element such as gold.

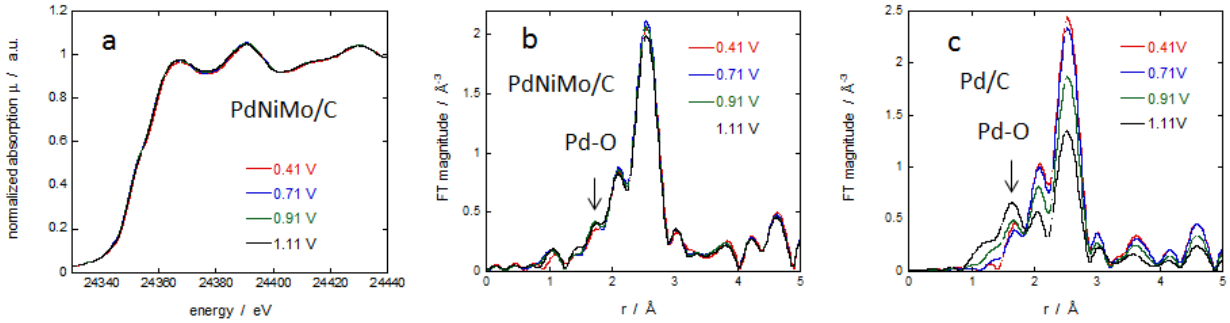


Figure 5. . *In situ* XANES (a) and FT-EXAFS (b) spectra of Pd K edge from PdNiMo/C in 1 M $HClO_4$ at different potentials. (c) *In situ* FT-EXAFS spectra of Pd K edge from a commercial Pd/C catalyst in 1 M $HClO_4$ at different potentials from Ref (22).

**Conclusions**

In this work, we synthesized Pt monolayer on ternary PdNiMo nanostructure core ($Pt_{ML}$/PdNiMo/C) electrocatalysts for the ORR by a sonochemical method. We used ionic liquid as a medium for functionalization and stabilizer of nanoparticles in an ethanol/water solvent, without the need of extra stabilizing molecules or organic solvents. The Pt specific and mass activities of the $Pt_{ML}$/PdNiMo/C electrocatalyst at 0.9 V are determined to be 0.55 $mA/cm^2$ and 1.14 $A/mg_{Pt}$, respectively, which are higher than those of a commercial Pt/C catalyst. The *in situ* XAS characterization studies by XAS show that the PdNiMo/C nanoparticles are very stable under potential up to 1.11 V, a value indicative of high tolerance of a Pt ML catalyst. The sonochemical synthesis also offers a less costly technique of making metal nanoparticles, thus making the process suitable for mass production.

**Acknowledgements**

The work at BNL was carried out with support from the U.S. Department of Energy, Office of Science, Division of Chemical Sciences, Geosciences & Biosciences, Office of Basic Energy Sciences under contract DE-SC0012704. DK acknowledge partial support as supplement grant from the National Science Foundation (NSF) for the NSF-CREST Bioenergy Center (Grant No. HRD-124215) and DM for a subcontract from NC A&T University. The synthesis work for this research was performed at the Advanced Energy Research and Technology Center, Stony Brook University, Stony Brook, New York. Characterization and Electrochemical studies were conducted at Brookhaven National Laboratory, Upton, NY 11973 (Center for Functional Nanomaterials, Chemistry Departments.). Funding provided by the AGEPT and Turner Fellowships, Center for Inclusive Education, Stony Brook University and the Research Foundation of the State University of New York.

## References


1. A. Manthriram, A. V. Murugan, A. Sarkar and T. Muraliganth, *Energy & Environment Science*, **1**, 621 (2008).
2. X. Huang, Z. Zhao, L. Cao, Y. Chen, E. Zhu, Z. Lin, M. Li, A. Yan, A. Zettl, Y. M. Wang, X. Duan, T. Muelle and Y. Huan, *Science Magazine*, **348**, 1230 (2015).
3. J. D. Scholten, B. C. Leal and J. Dupont, *ACS Catal.*, **2**, 184 (2012).
4. A. Kraynov and T. E. Muller, in *Applications of Ionic Liquids in Science and Technology*, S. Handy Editor, INTECH Open Access Publisher (2011).
5. P. Migowski, G. Machado, S. Texeira, M. Alves, J. Morais, A. Traversec and J. Dupont, *Phys. Chem. Chem. Phys.*, **9**, 4814 (2007).
6. M. Prechtl, P. Campbell, J. Scholten, G. Fraser, G. Machado, C. Santini, J. Dupont and Y. Chauvinb, *Nanoscale*, **2**, 2601 (2010).
7. K. Schutte, A. Doddi, C. Kroll, H. Meyer, C. Wiktor, C. Gemel, G. Tendeloo, A. Fischer and C. Janiak, *Nanoscale*, **6**, 5532 (2014).
8. C. Janiack, *Top. Organomet. Chem.*, **51**, 17 (2015).
9. K. S. Suslick, T. Hyeon and M. Fang, *Chemical Mater.*, **8**, 2172 (1996).
10. Y. Mizukoshi, T. Fujimoto, Y. Nagata, R. Oshima and Y. Maeda, *Journal of Physical Chemistry, B*, **104**, 6028 (2000).
11. A. Sarkar, V. Murugan and A. Manthiram, *J. Phys. Chem. C*, **112**, 12037 (2008).
12. N. Kakati, J. Maiti, S. H. Lee and Y. S. Yoon, *International Journal of Hydrogen Energy* **37**, 19055 (2012).
13. R. Venkatesan, M. H. Prechtl, J. D. Scholten, R. P. Pezzi, G. Machadoc and J. Dupont, *Journal of Material Chemistry*, **21**, 3030 (2011).
14. F. C. Oliveira, F. B. Effenberger, M. H. Sousa, R. F. Jardim, P. K. Kiyohara, J. Dupont, J. C. Rubim and L. M. Rossi, *Phys Chem Chem Phys*, **13**, 13558 (2011).
15. C. U. Okoli, K. A. Kuttiyiel, J. Cole, J. McCutchen, H. Tawfik, R. R. Adzic and D. Mahajan, *Ultrason Sonochem*, **41**, 427 (2018).
16. C. Atzori, G. C. Shearer, L. Maschio, B. Civalleri, F. Bonino, C. Lamberti, S. Svelle, K. P. Lillerud and S. Bordiga, *J Phys Chem C*, **121**, 9312 (2017).

17. D. S. Silvester, W. S. He, L. Aldous, C. Hardacre and R. G. Compton, *J Phys Chem C*, **112**, 12966 (2008).

18. R. R. Adzic, J. Zhang, K. Sasaki, M. B. Vukmirovic, M. Shao, J. X. Wang, A. U. Nilekar, M. Mavrikakis, J. A. Valerio and F. Uribe, *Top Catal*, **46**, 249 (2007).

19. B. Ravel, Newville, M. , *Synchrotron Radiat.* , **12**, 537 (2005).

20. C. Janiak, *Z Naturforsch B*, **68**, 1059 (2013).

21. C. Janiak, *Top Organometal Chem*, **51**, 17 (2015).

22. K. Sasaki, H. Naohara, Y. M. Choi, Y. Cai, W.-H. Chen, P. Liu and R. R. Adzic, *Nat. Commun.*, **3**, 1115 (2012).

23. S. J. George, O. B. Drury, J. Fu, S. Friedrich, C. J. Doonan, G. N. George, J. M. White, C. G. Young and S. P. Cramer, *J. Inorg. Biochem.*, **103**, 157 (2009).

24. W.-F. Chen, K. Sasaki, C. Ma, A. I. Frenkel, N. Marinkovic, J. T. Muckerman, Y. Zhu and R. R. Adzic, *Angew. Chem. Int. Ed.*, **51**, 6131 (2012).

25. M. Antonietti, D. Kuang, B. Smarsly and Y. Zhou, *Angew. Chem. Int. Ed.*, **43**, 4988 (2004).

26. J. H. Bang and K. S. Suslick, *Adv. Mater.*, **22**, 1039 (2010).

27. N. A. Anastasijevic, V. Vesovic and R. R. Adzic, *Journal of Electroanalytical Chemistry*, **229**, 305 (1987).

28. G. Y. Chen, K. A. Kuttiyiel, D. Su, M. Li, C. H. Wang, D. Buceta, C. Y. Du, Y. Z. Gao, G. P. Yin, K. Sasaki, M. B. Vukmirovic and R. R. Adzic, *Chem Mater*, **28**, 5274 (2016).

29. K. A. Kuttiyiel, K. Sasaki, D. Su, M. B. Vukmirovic, N. S. Marinkovic and R. R. Adzic, *Electrochimica Acta*, **110**, 267 (2013).

30. Y. Lu, Y. Jiang and W. Chen, *Nano Energy*, **2**, 836 (2013).

31. J. Zhang, K. Sasaki, E. Sutter and R. R. Adzic, *Science*, **315**, 220 (2007).

32. K. Sasaki, H. Naohara, Y. Cai, Y. M. Choi, P. Liu, M. B. Vukmirovic, J. X. Wang and R. R. Adzic, *Angew. Chem. Int. Ed.*, **49**, 8602 (2010).